Editors' Suggestion

Field-induced insulating states in a graphene superlattice

S. Pezzini,[1,2,*] S. Wiedmann,[1,2] A. Mishchenko,[3] M. Holwill,[3] R. Gorbachev,[3] D. Ghazaryan,[3,4] K. S. Novoselov,[3] and U. Zeitler[1,2]

[1]*High Field Magnet Laboratory (HFML-EMFL), Radboud University, NL-6525 ED Nijmegen, Netherlands*
[2]*Institute for Molecules and Materials, Radboud University, NL-6525 AJ Nijmegen, Netherlands*
[3]*School of Physics and Astronomy, University of Manchester, Oxford Road, Manchester M13 9PL, United Kingdom*
[4]*Department of Physics, National Research University Higher School of Economics, Staraya Basmannaya 21/4, Moscow 105066, Russian Federation*

(Received 26 October 2018; published 29 January 2019)

We report on high-field magnetotransport (B up to 35 T) on a gated superlattice based on single-layer graphene aligned on top of hexagonal boron nitride. The large-period moiré modulation (≈15 nm) enables us to access the Hofstadter spectrum in the vicinity of and above one flux quantum per superlattice unit cell ($\Phi/\Phi_0 = 1$ at $B = 22$ T). We thereby reveal, in addition to the spin-valley antiferromagnet at $\nu = 0$, two insulating states developing in positive and negative *effective* magnetic fields from the main $\nu = 1$ and $\nu = -2$ quantum Hall states, respectively. We investigate the field dependence of the energy gaps associated with these insulating states, which we quantify from the temperature-activated peak resistance. Referring to a simple model of local Landau quantization of third-generation Dirac fermions arising at $\Phi/\Phi_0 = 1$, we describe the different microscopic origins of the insulating states and experimentally determine the energy-momentum dispersion of the emergent gapped Dirac quasiparticles.

DOI: 10.1103/PhysRevB.99.045440

I. INTRODUCTION

Van der Waals assembly of atomically thin materials represents a novel powerful strategy for the realization of artificial structures with tailored electronic response [1]. Inherent in this approach is the control of the crystallographic orientation of the atomic layers, a novel degree of freedom that can profoundly alter the electrostatic landscape experienced by the charge carriers. The stack of graphene [2] on top of hexagonal boron nitride (hBN) [3] and the subsequent reconstruction of the electronic spectrum hosting "second-generation" Dirac cones [4] are a prototypical case. The small lattice mismatch (≈1.8%) between their isomorphic structures results in a hexagonal superlattice modulation (the so-called moiré pattern) [4–6], which sets an artificial periodicity as large as $\lambda \approx 15$ nm for perfect crystallographic alignment. This twist-dependent superstructure, combined with the possibility of *in situ* tuning of the band filling via the electrostatic field effect, has made graphene-hBN superlattices the ideal platform for the experimental study of the Hofstadter butterfly (HB) [7–10]. The HB is the fractal (i.e., recursive, self-similar) energy spectrum acquired by a two-dimensional (2D) electronic system when simultaneously subjected to (i) a periodic electrostatic potential (the hexagonal moiré in our case) and (ii) a perpendicular magnetic field [7]. A spatially periodic potential groups the electronic states into discrete Bloch bands [11]; a perpendicular magnetic field quantizes the electronic spectrum into Landau levels [12]. These fundamental effects can usually be treated independently; however, under particular circumstances the two quantizations combine into the HB. This happens when rational values of magnetic flux quanta ($\Phi_0 = h/e$) thread the superlattice unit cell, i.e., when $\Phi/\Phi_0 = BA/(h/e) = p/q$ (where Φ is the total magnetic flux, A is the superlattice unit cell area, h is the Planck constant, and e is the electron charge). Thereby, the Bloch (Landau) bands splits into q (p) subbands, leading to a repeated "cloning" of the original magnetic spectrum [7].

In the case of graphene superlattices, the HB combines with the specific response of graphene's 2D Dirac fermions to large magnetic fields [13,14]. When tuned to charge neutrality, graphene systems exhibit a field-induced insulating state which has been a subject of intensive experimental study in single layers [15–20], bilayers [21–25], and multilayers [26,27]. This state arises at half filling of the zero-energy Landau level (LL), a unique signature of Dirac fermions, and has an interaction-induced origin based on the so-called quantum Hall (QH) ferromagnetism (QHFM), i.e., on the formation of spin-valley polarized states at partial LL fillings [28]. It is therefore of fundamental interest to understand if "copies" of this state are present in graphene's HB and in what way their phenomenology differs from the "original" one. Using capacitance spectroscopy, Yu *et al.* already showed evidence for QHFM in graphene superlattices [29]. However, magnetocapacitance is sensitive only to the bulk density of states and does not allow discerning between QH and insulating states. On the other hand, electrical transport can be employed to identify insulating phases with an energy gap for both the bulk and edge excitations. Bearing this in mind, we have investigated a 15-nm graphene-hBN superlattice with high-field,

*Present address: Center for Nanotechnology Innovation, NEST, Italian Institute of Technology, Piazza S. Silvestro 12, I-56127 Pisa, Italy; sergio.pezzini@iit.it

temperature-dependent magnetotransport measurements. By this means, we reveal three field-induced insulating states in the HB and quantitatively estimate their activation energies and the gaps' field dependence. Their microscopic origin is interpreted in connection with the emergence of so-called third-generation Dirac particles, i.e., a field- and superlattice-induced replica, experiencing zero effective magnetic field when $\Phi = \Phi_0$ (i.e., at $B = 22$ T for our superlattice). By analyzing their local Landau quantization, we reveal a significant renormalization in the Fermi velocity of the corresponding gapped Dirac cones.

II. EXPERIMENTAL METHODS

We studied a six-terminal Hall bar device ($W \times L = 1 \times 2\ \mu\text{m}^2$), defined by reactive ion etching and evaporation of Cr/Au contacts. The sample is based on a stack of single-layer graphene on top of a 50-nm-thick hBN crystal, obtained with a dry van der Waals assembly technique [30]. Straight edges of the two crystals are aligned within ≈1° during the assembly (giving a 50% success chance of crystallographic alignment due to the uncertainty of the zigzag or armchair nature of the selected edges). The measurements presented were performed in a ^{4}He-flow cryostat (base temperature of 1.5 K) inserted in the access bore of a resistive Bitter magnet at the High Field Magnet Laboratory (HFML-EMFL). The resistance was measured with low-frequency lock-in detection in both two- and four-probe configurations with a constant ac voltage of 10 mV applied to the sample connected in series to a 100-kΩ resistor.

III. RESULTS AND DISCUSSION

A. Hofstadter butterfly

The black trace in Fig. 1(a) shows the four-terminal resistance of our device R_{xx} as a function of gate voltage V_g (applied to the underlying Si/SiO_2 substrate), measured at $B = 0$ T and $T = 1.5$ K. As expected for an aligned graphene-hBN stack, three pronounced peaks are visible. At $V_g = V_g^{CNP} \approx 3$ V the Fermi level is set at the touching between the conduction and valence band Dirac cones. The peak value of the resistance at this point remains ≈10 kΩ (slightly varying over different cooldowns), indicating that no appreciable band gap opens in the absence of a magnetic field. The two additional maxima symmetrically located at large positive and negative doping $|\Delta V_g| = |V_g - V_g^{CNP}| = 32.5$ V, on the other hand, correspond to half filling of *second-generation* Dirac minibands induced by the superlattice potential [4]. To confirm this identification, we measured the Hall resistance R_{xy} as a function of V_g at low magnetic field ($B = 0.5$ T, avoiding quantization effects) and extracted the corresponding 2D carrier density $n(V_g) = B/(eR_{xy})$ [red open circles in Fig. 1(a)]. Close to $V_g = 0$ V, n changes its sign as the system is set to the charge neutrality point (CNP), while it varies linearly with V_g otherwise, with a slope $\alpha = 6.3 \times 10^{10}$ cm^{-2}/V. Farther away from the main CNP, n changes its sign the first time at the onset of the superlattice minibands ($|\Delta V_g| = 26$ V, corresponding to Van Hove singularities [31]) and a second time at $|\Delta V_g| = 32.5$ V, indicating the CNPs for the superlattice-induced Dirac

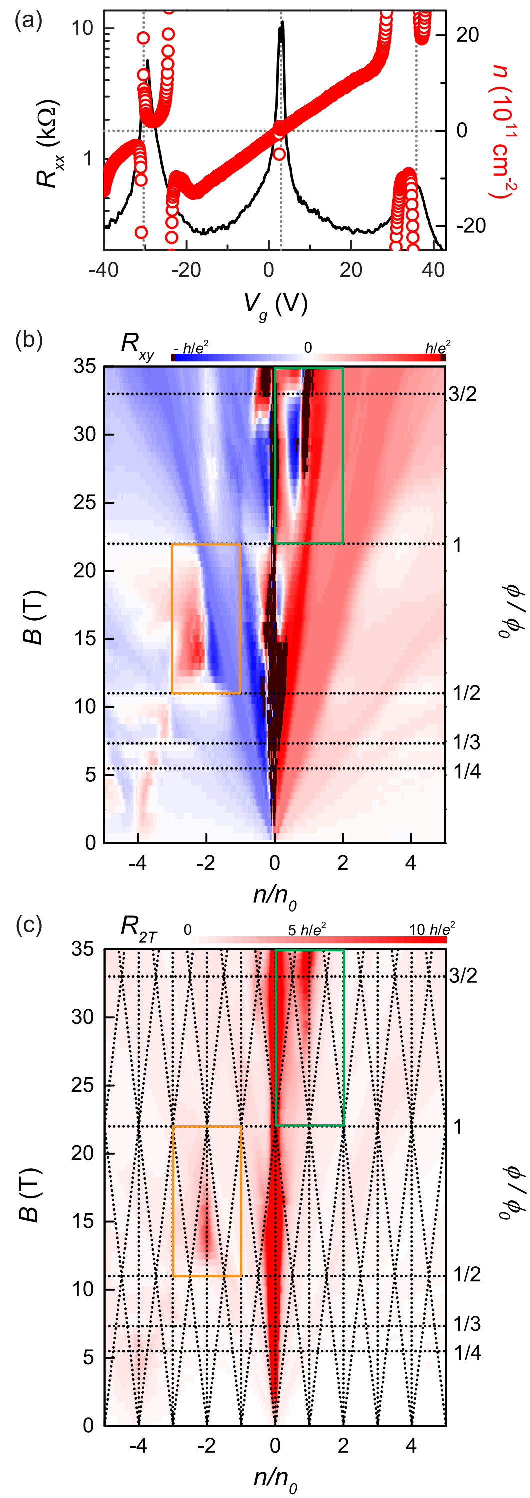

FIG. 1. (a) Black line: $R_{xx}(V_g)$ at $B = 0$ T. Red circles: $n(V_g)$, extracted from R_{xy} at $B = 0.5$ T. The vertical dotted lines indicate the main and satellite CNPs. (b) R_{xy} as a function of B and charge density per superlattice unit cell. On the right axis B is converted to Φ/Φ_0, with some rational values indicated. (c) R_{2T} over the same field and density ranges as in (b). The vertical (diagonal) dotted lines correspond to gaps in the Wannier diagram with index $t = 0$ ($t = \pm 1$). The maps were acquired as V_g sweeps at constant B, with 0.5 T steps; $T = 1.5$ K, unless otherwise specified. The green and orange rectangles mark the two regions discussed in Fig. 2.

minibands. Due to the spin and valley degeneracy, these satellite CNPs are realized when accommodating four electrons per superlattice unit cell, i.e., when $n = 4n_0 = 2.05 \times 10^{12}$ cm^{-2}, with $n_0 = 1/A = 2/(\sqrt{3}\lambda^2)$. The positioning of the satellite peaks therefore allows us to estimate a periodicity $\lambda = 15$ nm for the hexagonal moiré pattern, which confirms the high degree of crystallographic alignment between the graphene and hBN crystals.

In Fig. 1(b) we present a color map of the Hall resistance as a function of magnetic field (0 T $< B <$ 35 T) and carrier density per superlattice unit cell n/n_0 [corresponding to the same range of V_g used in Fig. 1(a)]. The red areas indicate electron doping, and the blue ones show hole doping, while in the black ones $|R_{xy}|$ exceeds h/e^2, typically signaling a divergence due to a CNP. On top of the standard Landau fan diagram of single-layer graphene (with full degeneracy lifting of the $N = 0$ LL), one can clearly identify a recursive pattern due to the HB. This is particularly evident in the lower left part of the map, which is dominated by a series of charge conversions and local Landau minifans. These features are understood in terms of the formation of q-fold-degenerate Zak minibands [32], which are, in fact, gapped Dirac cones [33], and experience zero effective field B_{eff} when $\Phi/\Phi_0 = p/q$. The emergent *third-generation* Dirac quasiparticles are then subjected to Landau quantization in a finite (positive or negative) effective magnetic field $B_{\text{eff}} = B - \Phi_0 Ap/q$. The appearance of these structures has a clear $1/B$ periodicity, with a characteristic frequency $f = \Phi_0/A = 22$ T, that provides an alternative way to estimate the moiré periodicity $\lambda = 14.7$ nm, in reasonable accordance with the value given above.

B. Insulating regions within local Landau fans

Within the HB, a simple Diophantine relation $n/n_0 = t(\Phi/\Phi_0) + s$ (with t and s being integer numbers, although fractional indices were recently reported in Refs. [34,35]) locates the expected incompressible (i.e., bulk-gapped) states in the flux-density space. The slope t can be seen as a generalized filling factor and actually defines the expected Hall conductivity $\sigma_{xy} = t(e^2/h)$, while s indicates the amount of filling of the Bloch bands. In Fig. 1(c) we plot a grid of $n/n_0 = t(\Phi/\Phi_0) + s$ lines, i.e., a so-called Wannier diagram [36], limited to only $t = 0, \pm 1$, on top of a color map of the two-terminal resistance of our device R_{2T}. For convenience and better visibility we use R_{2T} (rather than the four-terminal resistance R_{xx}) in this color map; however, all the quantitative analysis later on will be performed using quantities not affected by the contact resistance, i.e., σ_{xx}, σ_{xy}, and R_{xx}. In this graph, we can conveniently identify different regions in the field-gate space in which the device becomes strongly resistive. These regions disperse as $t = 0$, i.e., as vertical lines in the Wannier diagram, and appear to be strongly modulated by the $|t| = 1$ gaps, which enclose regions of Landau filling <1. The first insulating area at $n/n_0 = 0$ (reaching a maximum two-terminal resistance $R_{2T}^{\max} = 8.4$ MΩ and four-terminal resistance $R_{xx}^{\max} = 2.6$ MΩ at $T = 1.5$ K) extends over the whole field range and corresponds to half filling of the main $N = 0$ LL. A second insulating state ($R_{2T}^{\max} = 0.5$ MΩ, $R_{xx}^{\max} = 0.3$ MΩ) is located at $n/n_0 = 1$ and develops for $B > 22$ T, i.e., in $B_{\text{eff}} = B - 22$ T > 0 (green box). A third (weaker) one ($R_{2T}^{\max} = 0.2$ MΩ, $R_{xx}^{\max} = 70$ kΩ) develops at $n/n_0 = -2$ for $B < 22$ T, i.e., for $B_{\text{eff}} < 0$ (orange box). From comparison with Fig. 1(b), it is evident that all three insulating states also correspond to changes in the sign of R_{xy}, marking the boundary between local electron-doped and hole-doped regions. However, not every change in the carrier sign corresponds to insulating regions: notably, the satellite neutrality points do not develop into a B-induced insulating state due to overlap with the robust Landau gaps from the main neutrality point. On the other hand, the B_{eff}-induced insulating states do not coexist with any state from the main QH fan, which makes them observable in our experiment. The competition with Landau gaps developing in the same field-density region evidently constrains the possibility to experimentally access the insulating states. In addition, our experiment reveals a pronounced electron-hole asymmetry in the HB [see Fig. 1(b)], clearly affecting the second and third insulating states, for which we did not find a particle-hole symmetric. This asymmetry was consistently seen in previous experiments on graphene-hBN superlattices [8–10] and was reproduced by calculations [31,33]. The superlattice perturbation induced by a hexagonal substrate with inequivalent sublattice sites (i.e., hosting boron and nitrogen atoms) is considered responsible for this effect [37].

In the following, we use the notation (ν, ν_L) [29] in order to label the incompressible states in the local fan diagrams and check the consistency of the two B_{eff}-induced insulating states within the Hofstadter picture. Here ν is the filling factor of the parent QH state, while ν_L is the filling factor in the local Landau fan. The relations $t = \nu + \nu_L$ and $s = -\nu_L$ necessarily hold. Figure 2(a) shows an enlarged view of the $n/n_0 = 1$, $B_{\text{eff}} > 0$ region, centered on the $(1, -1)$ insulating state. The index ν is given by the main QH state located at $n/n_0 = 1$ for $B = 22$ T, i.e., $\nu = 1$ (shaded area). This QH state determines the energy gap for the third-generation Dirac particles at $\Phi/\Phi_0 = 1$, $n/n_0 = 1$. The local QH fan, resulting from occupation of singly degenerate local LLs, is shown in Fig. 2(b) (along with the neighboring one, which develops from the main $\nu = 0$ state). The color code corresponds to the expected value for the Hall conductivity, given by $\sigma_{xy} = t(e^2/h)$ (gray $= 0$, dark blue $= -1$, dark red $= +1$, light blue $= -2$, light red $= +2$). Figure 2(c) shows line traces of σ_{xy} and σ_{xx} at $B = 30$ T ($B_{\text{eff}} = 8$ T), which matches the expectation of the local fan diagram in Fig. 2(b). Although this pattern was reproducible over several cooldowns, the accuracy in the quantization of σ_{xx} and σ_{xy} was found to vary as a result of thermal cycling [e.g., the state (0,1), which cannot be identified here, was close to quantization in a previous measurement session]. As shown in Figs. 2(d)–2(f), the same analysis is successfully applied to the $(-2, 2)$ insulating state in the $n/n_0 = -2$, $B_{\text{eff}} < 0$ region, which corresponds to a main filling factor $\nu = -2$, although the quantization at $B_{\text{eff}} = -7$ T is found to be generally less accurate than in the previous case.

C. Energy gaps and microscopic origin

Having rationalized the presence of the $(1, -1)$ and $(-2, 2)$ states in graphene's HB, it is worthwhile to compare our observations with the existing experimental literature on

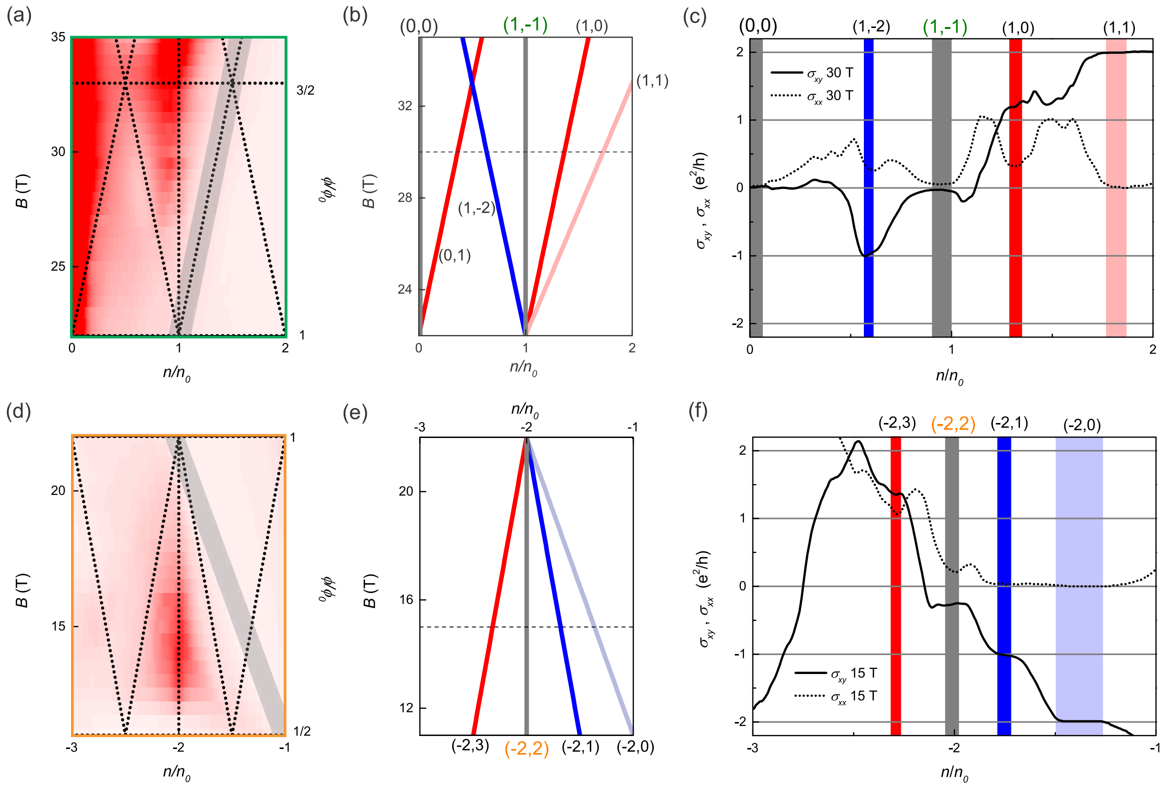

FIG. 2. (a) and (d) Enlarged plots of R_{2T} in the regions hosting the insulating states $(1,-1)$ and $(-2,2)$ [green and orange rectangles in Figs. 1(b) and 1(c)]. The shaded areas correspond to the parent QH states, $\nu=1$ and $\nu=-2$, respectively. (b) and (e) Local QH fan for the two regions in (a) and (d), labeled according to the notation (ν,ν_L) [29]. The colors indicate the expected Hall conductivity $\sigma_{xy}[(e^2/h)]=\nu+\nu_L$ (gray = 0, dark blue = -1, dark red = $+1$, light blue = -2, light red = $+2$). (c) and (f) σ_{xx} and σ_{xy} at the field indicated by the dashed lines in (b) and (e) over the same density range as in the other panels. The local QH states are highlighted by the same color code as in the diagrams in (b) and (e).

the subject. In particular, Yu *et al.* already identified both $(1,-1)$ and $(-2,2)$ states as incompressible in capacitance measurements [29], while Hunt *et al.* showed vanishing two-terminal conductance at both $(1,-1)$ and its particle-hole-symmetric $(-1,1)$ [10]. Moreover, by carefully inspecting the color plots in Ref. [34], one can spot an even larger number of such highly resistive regions. However, quantitative information on the amplitude of the energy gaps and its connection to the physical origin of these states is still missing. Therefore, we measured $R_{xx}(V_g)$ in the vicinity of the three insulating states (0,0), $(1,-1)$, and $(-2,2)$ for increasing temperatures and different magnetic fields, with steps of 1 T. Typical $R_{xx}(V_g)$ traces for the three states, at representative values of T and fixed B (B_{eff}), are plotted in Figs. 3(a)–3(c). The insulating temperature dependence, i.e., the peak in R_{xx} increasing with decreasing temperature and exceeding h/e^2, is evident in the three panels. We then analyzed these data by fitting an Arrhenius-type behavior $R_{xx}(T)=R_0\exp(\Delta/2k_BT)$ to the T dependence at fixed values of B (Δ is the energy gap, and k_B is the Boltzmann constant), which is clearly emphasized in $\ln(R_{xx})$ vs $1/T$ plots, as shown in Figs. 3(d)–3(f). Typically, this exponential dependence applies to relatively high temperature ranges, while R_{xx} saturates at low T, where it results from hopping between localized states inside the energy gap. In Fig. 3(g) we show the complete field dependence of the energy gaps of the three insulating states, obtained by fits of the kind shown by solid lines in Figs. 3(d)–3(f); the error bars are given by the standard error in the fitting parameter Δ. We discuss this panel by referring to the schematic diagram of Fig. 4, which shows a simple model of Landau quantization for the third-generation Dirac fermions and the resulting energy gaps [29,33]. The main LLs are represented as hatched areas; in accordance with the experimental observations [see Fig. 1(b)], the main $N=0$ LL splits into four branches, while the $N=-1$ LL retains the fourfold degeneracy. The states relevant to our discussion are color filled, with a code intended to match the plots in Fig. 2.

The (0,0) insulating state extends over the entire field range considered in our experiment. Its energy gap can be estimated to be on the order of 150 K (14 meV) already at $B=1$ T [see open circles in Fig. 3(g)]. This energy scale is well beyond the single-particle spin splitting determined by the Zeeman energy $E_Z=g\mu_BB\approx1.2\,[\mathrm{KT}^{-1}]\times B$ (where g is the Landé factor and μ_B is the Bohr magneton). It is instead comparable to the Coulomb energy $E_C=e^2/4\pi\epsilon_0\epsilon_rl_B\approx643/\epsilon_r\,[\mathrm{KT}^{-1/2}]\times\sqrt{B}$ (where l_B is the magnetic length and ϵ_r is the relative dielectric constant), which is plotted as a gray solid line in Fig. 3(g), assuming $\epsilon_r=5$ for the nonencapsulated graphene-hBN sample used in this experiment [38]. This observation is consistent with the formation of a spin-valley antiferromagnetic order at half filling of the $N=0$ LL [39], in which electrons with opposite spin polarizations occupy the

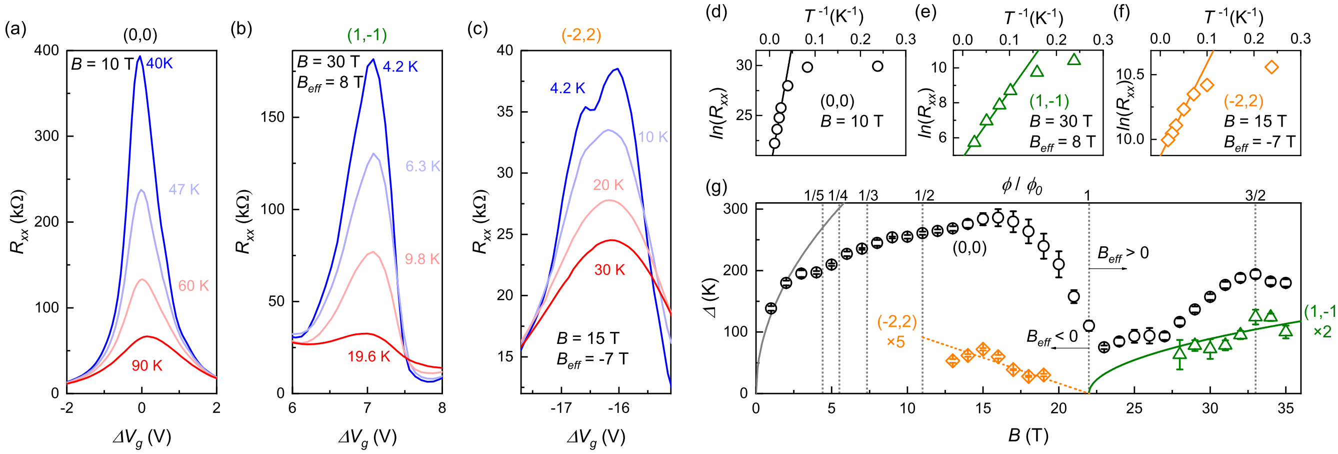

FIG. 3. (a)–(c) $R_{xx}(V_g)$ at selected temperatures corresponding to the three insulating states at representative values of the magnetic field. (d)–(f) Maxima of R_{xx} (in ln scale) as a function of $1/T$, extracted from V_g sweeps at constant B, such as the ones shown in (a)–(c). The solid lines are fit to the activation law $\ln(R_{xx})\alpha\Delta/2k_BT$. (g) The resulting energy gaps Δ are plotted in Kelvin units as a function of the magnetic field. The gray line represents the Coulomb energy, the green solid one is a $\sqrt{B_{\rm eff}}$ fit to $\Delta(1,-1)$, and the orange dashed one is a linear fit to $\Delta(-2,2)$ for $B_{\rm eff} < 0$. The data and fits for $\Delta(-2,2)$ and $\Delta(1,-1)$ are multiplied by a factor of 5 and 2, respectively.

two sublattice sites, minimizing the Coulomb repulsion [20]. The energy gap $\Delta(0,0)$ shows a markedly nonmonotonic behavior as a function of magnetic field: it grows in the range 1 T $< B <$ 16 T (although significantly deviating from E_C from 4 T on), strongly decreases for 16 T $< B <$ 22 T, and finally increases again up to the highest fields applied. We attribute the deviation from E_C to the fact that resistance data at relatively high temperature (up to $T = 90$ K) were necessary to estimate $\Delta(0,0)$. At such temperatures the Zak minibands arising at rational values of flux quanta, recently identified in a new kind of quantum oscillatory phenomenon [40,41], compete with the thermally excited conductivity across the gap, partially hindering the exponential dependence of R_{xx}. The dramatic suppression of the gap in the second region is due to the exponential broadening of the split LLs caused by the superlattice modulation, which reaches its maximum at $\Phi/\Phi_0 = 1$, where the band edges correspond to gapped Dirac cones [31]. Local LL quantization in $B_{\rm eff} > 0$ yields to the opening of a $\upsilon_L = 0$ state, which is reflected by the final increase in $\Delta(0,0)$. These findings are fully consistent with previous magnetocapacitance spectroscopy measurements [29].

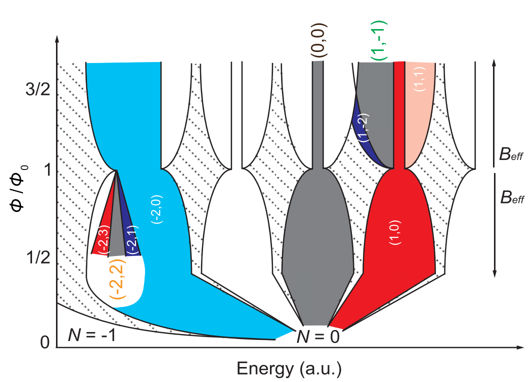

FIG. 4. Schematic diagram for the evolution of the relevant energy levels and gaps with Φ/Φ_0 and $B_{\rm eff}$. The superlattice-broadened $N=-1$ and (split) $N=0$ LLs are depicted as hatched areas, while the (ν,ν_L) states considered in our discussion are filled according to the color scale matching Figs. 1(b), 2(b), 2(c), 2(e), and 2(f).

The gap for the $(1,-1)$ insulating state [open green triangles in Fig. 3(g)] is sizable for $B > 27$ T ($B_{\rm eff} > 5$ T), increases monotonically with the field, and is best fitted by a $\sqrt{B_{\rm eff}}$ dependence. The parent quantum Hall state in this case is the $\nu = 1$, (1,0) in the local notation. Its gap is known to be determined by the energy cost of the formation of skyrmionic spin textures [28], which is proportional to E_C. The $\nu = 1$ is found to extend continuously from $B = 3$ T [see Fig. 1(b)] without experiencing any gap closing, which was instead reported at $\Phi/\Phi_0 = 1$ in Ref. [29]. The fact that (1,0) remains gapped at $B_{\rm eff} = 0$ [with $\delta(1,0)\,(B = 22\ {\rm T}) \approx 20$ K] is attributed to the smaller dielectric constant in our nonencapsulated sample, which enhances the interaction effects in comparison to the case of fully encapsulated structures ($\epsilon_r = 8$), like the capacitance device used in Ref. [29]. On the other hand, the $(1,-1)$ state results from full depletion of a singly degenerate $N = 0$-like local Landau level. Therefore, it is safe to assume that this insulating state has a single-particle origin, i.e., that it corresponds to the first cyclotron gap in the local singly degenerate Landau fan (see the corresponding gray area in Fig. 4), whose amplitude is given by $\upsilon_F^*\sqrt{2\hbar e B_{\rm eff}}$. Our best fit $\Delta(1,-1) = (15.7 \pm 0.8)$ [KT$^{-1/2}$] $\times\sqrt{B_{\rm eff}}$ can therefore provide a way to estimate the Fermi velocity of the corresponding third-generation Dirac fermions υ_F^*. However, it is well known that the experimental activation gap for the equivalent state in the conventional graphene spectrum ($\nu = -2$), although extremely large [42], highly underestimates the theoretical cyclotron gap. To circumvent this issue, we measured the activation gap of the $(-2,0)$ state in our sample at $B = 2$ T, where full quantization is already achieved and superlattice effects are minimized, and obtained $\Delta(-2,0)\,(B = 2\ {\rm T}) = 108$ K (theoretical value of 590 K). We then estimated υ_F^* from the ratio $[\Delta(1,-1)/\sqrt{B_{\rm eff}}]/[\Delta(-2,0)/\sqrt{B}]$. The direct comparison between two states with the same microscopic origin, i.e., the first cyclotron gap in the Dirac spectrum, in effective and absolute fields is intended to take into account the

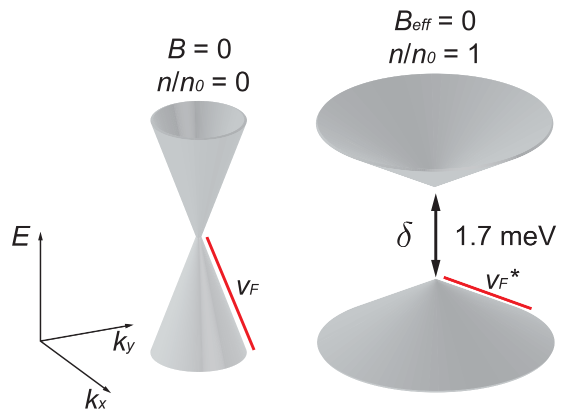

FIG. 5. Comparison between the energy-momentum dispersion of Dirac fermions close to half filling in single-layer graphene (left) and the field-induced third-generation ones at $\Phi/\Phi_0 = 1$, $n/n_0 = 1$ in a graphene superlattice (right). The cones' energy dispersions are given by $\pm v_F \hbar \sqrt{k_x^2 + k_y^2}$ and $\pm[\delta/2 + v_F^* \hbar \sqrt{k_x^2 + k_y^2}]$, respectively. The energy gap δ is determined by the $\nu = 1$ broken-symmetry QH state at 22 T. The Fermi velocity $v_F^* = 0.2 v_F$ is quantitatively estimated by comparing the field-dependent energy gap of the insulating state $(1, -1)$ with its analogous $\nu = -2$ in the main QH fan.

sample-dependent localization mechanism that is responsible for the bulk gaps in the quantum Hall regime. Our analysis gives $v_F^* \approx 0.2 v_F$; that is, it indicates a significant renormalization of the band dispersion for the field- and superlattice-induced Dirac fermions with respect to the ones of standard single-layer graphene ($v_F = 10^6$ m/s). A schematic comparison is presented in Fig. 5.

Finally, the field dependence of the activation gap for the $(-2, 2)$ state is presented as open orange diamonds in Fig. 3(g). This state appears to be less robust than the ones discussed above. This is reflected by its complete suppression at $\Phi/\Phi_0 = 1/2$, while the other insulating states remain sizable at $\Phi/\Phi_0 = 3/2$ and beyond. The single (quasi)quantized steps of σ_{xy} in the vicinity of $(-2, 2)$ [see Fig. 2(f)] indicate that the degeneracy of the fourfold local $N = 0$ LL for the replica Dirac fermions is fully lifted in negative B_{eff} (see Fig. 4). The $(-2, 2)$ state corresponds to half filling of this level; that is, it is analogous to the (0,0) state presented above. However, its gap is far from being comparable to E_C, and it is best fitted by $\Delta(-2, 2) = (1.7 \pm 0.1)\ [\text{KT}^{-1}] \times B_{\text{eff}}$, which can be attributed to Zeeman splitting in an effective magnetic field, with an enhanced Landé factor $g^* \approx 2.8$. This kind of B dependence of the gap at half filling of the $N = 0$ LL has typically been reported for disordered graphene samples on SiO_2 [17], while a much larger renormalized g^* was estimated for graphene on hBN in Ref. [28]. Despite the low-disorder environment guaranteed by the graphene/hBN stack, our observations indicate a moderate contribution of *e-e* interaction to the degeneracy lifting in this local Landau fan. Further experimental data would be, however, necessary to determine the exact microscopic ordering underlying the $(-2, 2)$ state; tilted-field experiments allowing for an independent tuning of the Zeeman field could be of particular relevance.

IV. CONCLUSIONS AND OUTLOOK

In summary, we have presented a study of temperature-dependent magnetotransport on a graphene-hBN superlattice with 15-nm moiré periodicity. The electrical transport experiments allow the identification of three fully gapped regions in the HB. These states, despite sharing a common insulating nature, can be traced to different microscopic origins within the main QH spectrum of single-layer graphene and its replica in the vicinity of $\Phi/\Phi_0 = 1$ ($B = 22$ T). Importantly, our analysis identifies the insulating state $(1, -1)$ as corresponding to the first cyclotron gap in the local Landau fan of the replica Dirac fermions. The B_{eff} dependence of its gap, in combination with knowledge of the $\nu = 1$ gap at 22 T, enables us to experimentally determine the energy-momentum dispersion of the corresponding superlattice- and field-induced third-generation quasiparticles. An extension of this quantitative approach to samples with different moiré lengths should elucidate the role of the superlattice periodicity in the renormalization of the replica spectrum. Continuous tuning of the graphene-hBN misalignment via the method of Ref. [43] could be used for the creation of Dirac particles with on-demand Fermi velocity and gap size.

ACKNOWLEDGMENTS

This work is part of Research Program No. 132 High Field Magnet Laboratory: a global player in science in high magnetic fields, financed by the Netherlands Organisation for Scientific Research (NWO). A.M. acknowledges the support of EPSRC Early Career Fellowship EP/N007131/1.

[1] A. K. Geim and I. V. Grigorieva, Nature (London) **499**, 419 (2013).
[2] K. S. Novoselov, A. K. Geim, S. V. Morozov, D. Jiang, Y. Zhang, S. V. Dubonos, I. V. Grigorieva, and A. A. Firsov, Science **306**, 666 (2004).
[3] C. R. Dean, A. F. Young, I. Meric, C. Lee, L. Wang, S. Sorgenfrei, K. Watanabe, T. Taniguchi, P. Kim, K. L. Shepard, and J. Hone, Nat. Nanotechnol. **5**, 722 (2010).
[4] M. Yankowitz, J. Xue, D. Cormode, J. D. Sanchez-Yamagishi, K. Watanabe, T. Taniguchi, P. Jarillo-Herrero, P. Jacquod, and B. J. LeRoy, Nat. Phys. **8**, 382 (2012).
[5] J. Xue, J. Sanchez-Yamagishi, D. Bulmash, P. Jacquod, A. Deshpande, K. Watanabe, T. Taniguchi, P. Jarillo-Herrero, and B. J. LeRoy, Nat. Mater. **10**, 282 (2011).
[6] R. Decker, Y. Wang, V. W. Brar, W. Regan, H.-Z. Tsai, Q. Wu, W. Gannett, A. Zettl, and M. F. Crommie, Nano Lett. **11**, 2291 (2011).
[7] D. Hofstadter, Phys. Rev. B **14**, 2239 (1976).
[8] L. A. Ponomarenko, R. V. Gorbachev, G. L. Yu, D. C. Elias, R. Jalil, A. A. Patel, A. Mishchenko, A. S. Mayorov, C. R. Woods, J. R. Wallbank, M. Mucha-Kruczynski, B. A. Piot, M. Potemski, I. V. Grigorieva, K. S. Novoselov, F. Guinea, V. I. Fal'ko, and A. K. Geim, Nature (London) **497**, 594 (2013).

[9] C. R. Dean, L. Wang, P. Maher, C. Forsythe, F. Ghahari, Y. Gao, J. Katoch, M. Ishigami, P. Moon, M. Koshino, T. Taniguchi, K. Watanabe, K. L. Shepard, J. Hone, and P. Kim, Nature (London) **497**, 598 (2013).

[10] B. Hunt, J. D. Sanchez-Yamagishi, A. F. Young, M. Yankowitz, B. J. LeRoy, K. Watanabe, T. Taniguchi, P. Moon, M. Koshino, P. Jarillo-Herrero, and R. C. Ashoori, Science **340**, 1427 (2013).

[11] N. W. Ashcroft and N. D. Mermin, *Solid State Physics* (Holt, Rinehart and Winston, New York, 1976).

[12] C. Kittel, P. McEuen, and P. McEuen, *Introduction to Solid State Physics* (Wiley, New York, 1996).

[13] K. S. Novoselov, A. K. Geim, S. V. Morozov, D. Jiang, M. I. Katsnelson, I. V. Grigorieva, S. V. Dubonos, and A. A. Firsov, Nature (London) **438**, 197 (2005).

[14] Y. Zhang, Y.-W. Tan, H. L. Stormer, and P. Kim, Nature (London) **438**, 201 (2005).

[15] Y. Zhang, Z. Jiang, J. P. Small, M. S. Purewal, Y.-W. Tan, M. Fazlollahi, J. D. Chudow, J. A. Jaszczak, H. L. Stormer, and P. Kim, Phys. Rev. Lett. **96**, 136806 (2006).

[16] J. G. Checkelsky, Lu Li, and N. P. Ong, Phys. Rev. Lett. **100**, 206801 (2008).

[17] A. J. M. Giesbers, L. A. Ponomarenko, K. S. Novoselov, A. K. Geim, M. I. Katsnelson, J. C. Maan, and U. Zeitler, Phys. Rev. B **80**, 201403(R) (2009).

[18] X. Du, I. Skachko, F. Duerr, A. Luican, and E. Y. Andrei, Nature (London) **462**, 192 (2009).

[19] G. L. Yu, R. Jalil, B. Belle, A. S. Mayorov, P. Blake, F. Schedin, S. V. Morozov, L. A. Ponomarenko, F. Chiappini, S. Wiedmann, U. Zeitler, M. I. Katsnelson, A. K. Geim, K. S. Novoselov, and D. C. Elias, Proc. Natl. Acad. Sci. USA **110**, 3282 (2013).

[20] A. F. Young, J. D. Sanchez-Yamagishi, B. Hunt, S. H. Choi, K. Watanabe, T. Taniguchi, R. C. Ashoori, and P. Jarillo-Herrero, Nature (London) **505**, 528 (2014).

[21] B. E. Feldman, J. Martin, and A. Yacoby, Nat. Phys. **5**, 889 (2009).

[22] F. Freitag, J. Trbovic, M. Weiss, and C. Schonenberger, Phys. Rev. Lett. **108**, 076602 (2012).

[23] J. Velasco, Jr., L. Jing, W. Bao, Y. Lee, P. Kratz, V. Aji, M. Bockrath, C. N. Lau, C. Varma, R. Stillwell, D. Smirnov, F. Zhang, J. Jung, and A. H. MacDonald, Nat. Nanotechnol. **7**, 156 (2012).

[24] P. Maher, C. R. Dean, A. F. Young, T. Taniguchi, K. Watanabe, K. L. Shepard, J. Hone, and P. Kim, Nat. Phys. **9**, 154 (2013).

[25] S. Pezzini, C. Cobaleda, B. A. Piot, V. Bellani, and E. Diez, Phys. Rev. B. **90**, 121404(R) (2014).

[26] W. Bao, L. Jing, J. Velasco, Jr., Y. Lee, G. Liu, D. Tran, B. Standley, M. Aykol, S. B. Cronin, D. Smirnov, M. Koshino, E. McCann, M. Bockrath, and C. N. Lau, Nat. Phys. **7**, 948 (2011).

[27] A. L. Grushina, D.-K. Ki, M. Koshino, A. A. L. Nicolet, C. Faugeras, E. McCann, M. Potemsk, and A. F. Morpurgo, Nat. Commun. **6**, 6419 (2015).

[28] A. F. Young, C. R. Dean, L. Wang, H. Ren, P. Cadden-Zimansky, K. Watanabe, T. Taniguchi, J. Hone, K. L. Shepard, and P. Kim, Nat. Phys. **8**, 550 (2012).

[29] G. L. Yu, R. V. Gorbachev, J. S. Tu, A. V. Kretinin, Y. Cao, R. Jalil, F. Withers, L. A. Ponomarenko, B. A. Piot, M. Potemski, D. C. Elias, X. Chen, K. Watanabe, T. Taniguchi, I. V. Grigorieva, K. S. Novoselov, V. I. Fal'ko, A. K. Geim, and A. Mishchenko, Nat. Phys. **10**, 525 (2014).

[30] A. V. Kretinin, Y. Cao, J. S. Tu, G. L. Yu, R. Jalil, K. S. Novoselov, S. J. Haigh, A. Gholinia, A. Mishchenko, M. Lozada, T. Georgiou, C. R. Woods, F. Withers, P. Blake, G. Eda, A. Wirsig, C. Hucho, K. Watanabe, T. Taniguchi, A. K. Geim, and R. V. Gorbachev, Nano Lett. **14**, 3270 (2014).

[31] J. R. Wallbank, A. A. Patel, M. Mucha-Kruczynski, A. K. Geim, and V. I. Fal'ko, Phys. Rev. B. **87**, 245408 (2013).

[32] J. Zak, Phys. Rev. **134**, A1602 (1964).

[33] X. Chen, J. R. Wallbank, A. A. Patel, M. Mucha-Kruczynski, E. McCann, and V. I. Fal'ko, Phys. Rev. B **89**, 075401 (2014).

[34] L. Wang, Y. Gao, B. Wen, Z. Han, T. Taniguchi, K. Watanabe, M. Koshino, J. Hone, and C. R. Dean, Science **350**, 1231 (2015).

[35] E. M. Spanton, A. A. Zibrov, H. Zhou, T. Taniguchi, K. Watanabe, M. P. Zaletel, and A. F. Young, Science **360**, 62 (2018).

[36] G. H. Wannier, Phys. Status Solidi B **88**, 757 (1978).

[37] A. M. DaSilva, J. Jung, S. Adam, and A. H. MacDonald, Phys. Rev. B **91**, 245422 (2015).

[38] C. R. Dean, A. F. Young, P. Cadden-Zimansky, L. Wang, H. Ren, K. Watanabe, T. Taniguchi, P. Kim, J. Hone, and K. L. Shepard, Nat. Phys. **7**, 693 (2011).

[39] M. Kharitonov, Phys. Rev. B. **85**, 155439 (2012).

[40] R. Krishna Kumar, X. Chen, G. H. Auton, A. Mishchenko, D. A. Bandurin, S. V. Morozov, Y. Cao, E. Khestanova, M. B. Shalom, A. V. Kretinin, K. S. Novoselov, L. Eaves, I. V. Grigorieva, L. A. Ponomarenko, V. I. Fal'ko, and A. K. Geim, Science **357**, 181 (2017).

[41] R. Krishna Kumar, A. Mishchenko, X. Chen, S. Pezzini, G. H. Auton, L. A. Ponomarenko, U. Zeitler, L. Eaves, V. I. Fal'ko, and A. K. Geim, Proc. Natl. Acad. Sci. USA **115**, 5135 (2018).

[42] K. S. Novoselov, Z. Jiang, Y. Zhang, S. V. Morozov, H. L. Stormer, U. Zeitler, J. C. Maan, G. S. Boebinger, P. Kim, and A. K. Geim, Science **315**, 1379 (2007).

[43] R. Ribeiro-Palau, C. Zhang, K. Watanabe, T. Taniguchi, J. Hone, and C. R. Dean, Science **361**, 690 (2018).